Infrared antenna metrology

5 authors, including:

Tasneem Mandviwala
Halliburton
3 PUBLICATIONS **35** CITATIONS

SEE PROFILE

Javier Alda
Complutense University of Madrid
187 PUBLICATIONS **1,721** CITATIONS

SEE PROFILE

Brian Lail
Florida Institute of Technology
95 PUBLICATIONS **680** CITATIONS

SEE PROFILE

Some of the authors of this publication are also working on these related projects:

Plasmonic Resonant Structures for solar cells and sensors View project

Fabrication and applications of planar nanoantennas View project

Infrared antenna metrology

José Manuel López-Alonso,[1] Tasneem Mandviwala,[1] Javier Alda,[2] B. Lail [1] and Glenn Boreman.[1]

[1] College of Optics and Photonics, CREOL, University of Central Florida,
Orlando, FL USA 32816-2700
E-mail:
joselope@creol.ucf.edu;tmandviwa@creol.ucf.edu:monacelli@creol.ucf.edu;blail@creo.ucf.edu
boreman@creol.ucf.edu

[2] School of Optics, University Complutense of Madrid.
Av. Arcos del Jalón, s/n, 28037, Madrid, Spain
Phone: +34 91 394 6874, Fax: +34 91 394 6885
E-mail: j.alda@fis.ucm.es

Abstract

Infrared antennas are a novel type of detectors that couples electromagnetic radiation into metallic structures and feed it to a rectifying element. As their radio and millimeter counterparts, they can be characterized by parameters explaining their response in a variety of situations. The size of infrared antennas scales with the detected wavelength. Then, specifically designed experimental set-ups need to be prepared for their characterization. The measurement of the spatial responsivity map of infrared antennas is one of the parameters of interest, but other parameters can be defined to describe, for example, their directional response, or polarization response. One of the inputs to measure the spatial responsivity map is the spatial distribution of the beam irradiance illuminating the antenna-coupled detector. The measured quantity is actually a map of the response of the detector when it moves under the beam illumination. This measurement is given as the convolution of the actual responsivity map and the beam irradiance distrbution. The uncertainties, errors, and artifacts incorporated along the measurement procedure are analyzed by using the Principal Component Analysis (PCA). By means of this method is possible to classify different sources of uncertainty. PCA is applied as a metrology tool to characterize the accuracy and repeatability of the experimental set-up. Various examples are given to describe the application of the PCA to the characterization of the deconvolution procedure, and to define the responsivity and the signal-to-noise ratio of the measured results.

1. Introduction.

Infrared antennas are novel detectors with promising applications. The principle is the same as the classical antennas working at larger than optical wavelengths (millimeter waves, radio waves). A metal structure with a size comparable to the radiation wavelength can convert the electromagnetic radiation into an electrical current. In the case of infrared and visible wavelengths, the size ranges from some microns down to a few hundreds of nanometers. This inspires the terms micro- and

nano-antennas when these devices are named. At the same time, the manufacture and testing procedures are falling in the scope of nanotechnology.

Used as a radiation detector, the applications are very appealing, from pixels for imaging applications in the infrared to biological sensors and so on.[1] At the same time, optical and infrared antennas behaves different than the conventional semiconductor detector. Due to the high frequency of the optical radiation at infrared and visible wavelengths, it is not possible to detect the excited current directly. For infrared and optical antennas the electric current is rectified and converted into a signal proportional to the energy falling onto the antenna. Two types of rectifying mechanism have been used so far: metal-oxide-metal diodes, and microbolometers. Specially interesting are the microbolometer antenna-coupled devices. The temporal response of these devices is related with its volume. The microbolometers can respond very fast to the incoming radiation, but the responsivity is low. The presence of the antenna increases its responsivity while maintaining the fast response.[2,3] Moreover, due to the use of an antenna to collect the incoming radiation, these detectors respond with strong dependence to the polarization and direction of light.

The small size of these devices imposes the development of special techniques to characterize and compare them with the results obtained from simulations. In this paper are described some techniques used to measure the response of the devices while presenting some of them.

2. Experimental set up.

A scheme of the experimental set up is shown in figure 1. A CO_2 infrared laser is used the illumination source. In our case, the laser wavelength can be tuned and monitored with a laser wavemeter. The laser signal is controlled with a reference detector and the polarization is set with a polarizer and a half-wave plate. The polarizer also controls the power delivered to the detector, and the half-wave plate rotates the plane of the linear polarized infrared laser. The radiation is mechanically modulated at a frequency of 2500 Hz and it is expanded and focused onto the detector with the help of infrared optics.
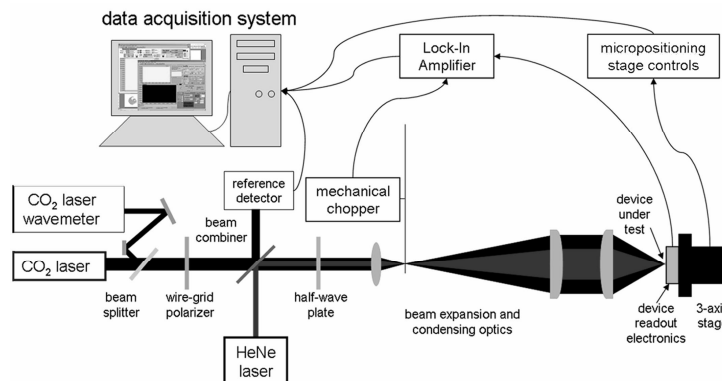

Figure 1: Scheme of the experimental set up used.

Two types of focusing elements are used. One of them is a F#1 lens that produce a tightly focused beams, close to the diffraction limit (around 30 microns). This beam is preferred when high accuracy spatial responsivity maps are needed. The other lens is a F#8 lens that provides with a wide focused beam, more appropriate for some other measurements.

2. Devices under tests.

We have used two different types of detectors: an antenna-coupled microbolometer system, and a dipole antenna connected to a coplanar stripline type transmission line and a microbolometer.

Infrared focal plane arrays can be fabricated consisting of antenna elements incoherently connected in serie.[4] With this interconnection, the current-wave from individual sensors adds up, but phase information across the array is not preserved. Hence this IR antenna would not work as a phased array antenna. The advantages of a phased array antennas is that the reception beam narrows as the array gets larger and the reception beam can be steered by controlling the phase difference between individual antennas. This has motivated the study of the interconnection suitable for IR-frequency current waves that will add each antenna's current together with preservation of phase information. The resulting aggregate current would then be sensed with a single sensor

We demonstrate the first LWIR transmission line design and characterization. No previous efforts have been made to study the performance of any transmission lines in IR frequency range. Frequency range above a couple of hundreds of GHz well exceed the range of validity of the quasi-static approximations that are often made in modeling the propagation of electrical signals on transmission line interconnects.[5] Numerical modeling is necessary for characterization of transmission lines at IR. We have characterized coplanar striplines (CPS) at IR frequency (28.3 THz) in terms of transmission line parameters: characteristic impedance (Z_o), attenuation constant (α) and phase constant (β).[6] The second type of device is described in reference 7.
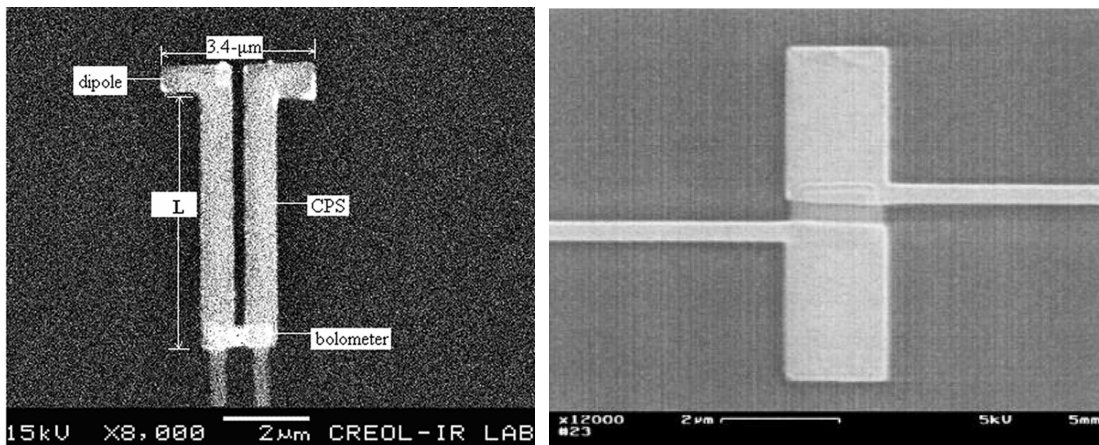

Figure 2: SEM micrographs of fabricated devices. Dipole antenna connected to a coplanar stripline type transmission line (left) and microbolometer coupled antenna (right).

3. Responsivity and polarization measurements.

We measured some important figures of merit over an infrared-frequency coplanar stripline. The experimental set up is the same as the one used in the previous measurements of this device (see figure 2). The only change has been the introduction of a LabView instrument to take the locking output with the computer. This permits to capture not only a point but a series of measurements in order to make statistical analysis. The equipment provides with data at a rate of approximately 0.3 seconds. A F#8 configuration is used that makes easy to locate the detector signal in space. The two parts of the optical system are calibrated in the following manner:

a) Polarizer and wave plate: this part of the setup is used to produce different signal levels changing the angle of the polarizer respect to the maximum signal orientation (θ_{max}). The signal after both optical elements is taken with the laser head and sent to a multimeter. Two hundred consecutive measurements are taken and the signal respect to angle $S\theta_{max}$ is taken as the mean value. The uncertainty $u^2(S\theta_{max})$ is calculated as:

$$u^2(S\theta_{max}) = \sigma^2 + (0.002 S\theta_{max})^2 + (0.0000155 S\theta_{max})^2 \cong \sigma^2 + (0.002 S\theta_{max})^2 \,(1),$$

where σ^2 is the variance of the measurements taken, and the rest of factors corresponds to the uncertainty in the head analog output and multimeter noise respectively. As it can be seen, the noise in the multimeter can be neglected. Finally, the signal in W ($P\theta_{max}$) is calculated using the conversion factor of the laser head (k=200 mW/1 V). The expression of the power and uncertainties are then,

$$P\theta_{max} = kS\theta_{max}$$
$$u^2(P\theta_{max}) = k^2 u^2(S\theta_{max}) \qquad . \qquad (2)$$

With this in mind, the Power in modeled as:

$$P\theta_{max} = m\cos^2\theta_{max} + b \rightarrow \begin{cases} m = 86.02 \pm 2.4 \\ b = -2.56 \pm 1.5 \end{cases}, \qquad (3)$$

with a 90% of probability. The values of *m* and *b* are calculated from a linear fitting of the data, taking into account the uncertainty in each measurement provided by equation (2).

b) The lens transmission is calculated in a similar way. The power is measured after and before the system of lenses, and it is expressed as a function of $\cos^2\theta_{max}$. This produces two different slopes, m_1 and m_2. The transmission T, and uncertainty can be calculated as:

$$T = \frac{m_1}{m_2} \rightarrow \left(\frac{u(T)}{T}\right)^2 = \left(\frac{u(m_1)}{m_1}\right)^2 + \left(\frac{u(m_2)}{m_2}\right)^2 . \qquad (4)$$

The results give a transmission of 0.912 ± 0.014 with a 95% of probability.

With the previous equation, an estimation of the value and uncertainty of the power falling onto the antenna can be calculated. The Signal Transfer Function (SiTF) is defined as:

$$SiTF = \frac{dV}{dP} \qquad . \qquad (5)$$

In this equation, V is the DC voltage given by the device, and P is the delivered optical power at the antenna plane. This definition of the SiTF is well suited in case some radiometric inaccuracies are present. There are two typical ways to measure this figure of merit. One of them is to approximate the derivative by a ratio of discrete increments $\Delta V / \Delta P$. A second more accurate way is to acquire several pairs of Voltage versus Power (V_i, P_i), then fit the resulting curve, and finally calculate the derivative at each point. Usually, the fitted dependence is linear and the SiTF can be seen as the slope of it. This will be the approach used in this paper. From it, we can obtain uncertainties values using the uncertainties of the fitting parameters.

In order to produce different power values we rotate the polarizer with respect to the polarization angle of the radiation coming from the laser. Then, we rotate the $\lambda/2$ wave plate in order to maintain the previous polarization angle respect to the device. Then, what is changed is $P\theta_{max}$. The polarization angles (θ) are 0, 10, 20, 30, 40, 50 where a zero angle means horizontal polarization. Some of the results are given in figure 3.
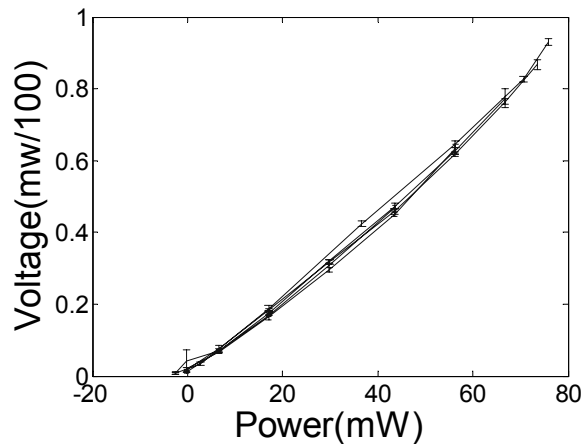

Figure 3: Plot of Voltage vs Power for different polarization angles.

As previously reported, the SiTF does not change significatively with polarization angle.[6] More analysis of this dependence is given in the next figures. Figure 4 shows the SiTF as a function of the angle of polarization. The difference in the response is small (see the vertical range), and it decays very fast after 30 degrees.
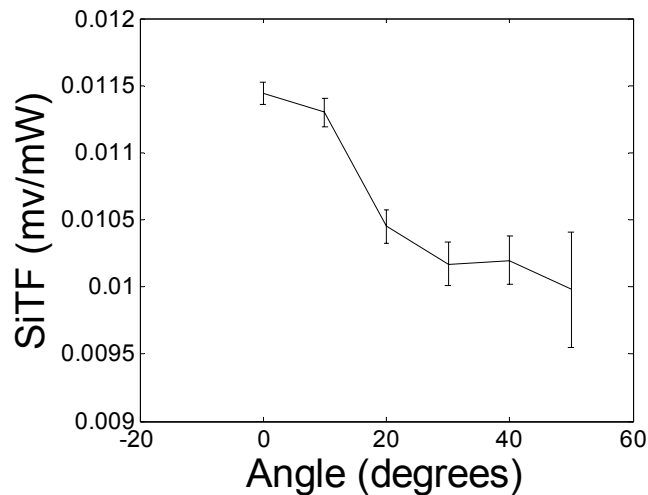
Figure 4: Plot of the SiTF as a function of angle of polarization.

3. Spatial response measurements and electrical efficiency.

The effective area of an antenna is a very important figure of merit. An antenna can collect radiation over a space region larger than its physical size. The relation of effective area to size can change depending of the design parameters. The general approach to measure the spatial response of the antenna detector is to scan it with a laser signal of known shape. The result can be seen as the convolution of the laser beam shape with the spatial response of the antenna.[8] Then, the spatial response can be calculated through an iterative deconvolution process. This figure of merit is more demanding from an experimental point of view. First, the beam size has to be close to the expected effective area in order to obtain a correct response from the deconvolution algorithm. Second, the beam shape has to be measured with great accuracy. Third, the small beam size and detector size makes difficult the positioning of the detector itself in the lens focal region. And fourth, the signals are weak. This compels us to consider special signal processing techniques to enhance and separate real signal from noise. In the following, we comment the principal factors in this type of measurements.

3.1 Beam shape characterization.

For the measurement of spatial response, a F#1 optics configuration is used. With an aperture of five centimeters, the diffraction limit beam size is around thirty microns for 10 microns wavelength. This makes impossible the characterization of beam shape by means of imaging techniques. A knife edge scan method is used instead. A knife edge coupled to a large area detector scans the focal region of the lens with a resolution of microns. Each scan is derived in order to obtain the integrated beam profile at that location. Looking at the whole set of scans it is possible to locate the focal point as the point where the beam waist is minimum and the signal is maximum. The main problem with this technique is the influence of noise on the measured data. Noise comes not only from the acquisition system, but from the laser itself. Infrared lasers tend to be not very stable and the signal power is affected mainly by changes in the temperature of laser. We have analyzed these signal fluctuations in a previous contribution.[9]

The noise problems are dealt with a signal processing technique called Principal Component Analysis (PCA) that has been applied to different types of noise filtering.[10,11] The principal features of this technique is explained in the next subsection.

3.2 Principal Component Filtering

Basically, PCA is a statistical multivariate technique that permits to organize and filter a collection of multivariate data. In our case, each scan is taken as a random variable due to noise. Then, the covariance matrix among them is calculated. This matrix is diagonalized by calculating the eigenvalues and eigenvectors. Eigenvectors can be seen as a new base for the original scan. Transforming them to the new base, makes them uncorrelated. The original data in the new base are called Principal Components. The principal application of this transformation is that, usually, noise, signal and other artifacts have a different degree of correlation. Decomposing this correlation with PCA allows an easy identification and sorting of them. The next step is to remove the noise components of the signal and then transforms it to the original base. This process is called PCA rectification[10,11]. The filtering process takes into account the total correlation information of the signal, and therefore the signal information content is recovered with high accuracy. Moreover, because of that, the procedure can be applied to different systems and data sets.
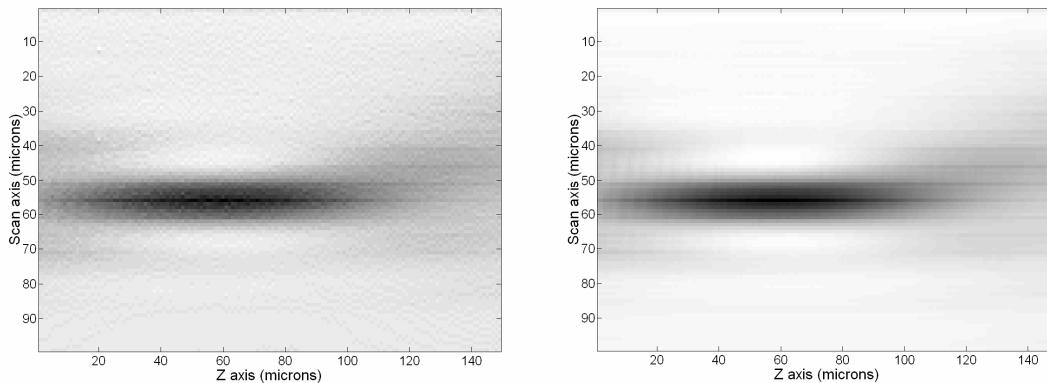

Figure 5: Noise filtering applied to a set of derived knife edge scan data set. Without filtering (left), after filtering (right).

3.3 Spatial response

After properly locating the position of best focus, the same procedure is applied to horizontal and vertical directions. The two laser scans are used to calculate the beam shape through a fitting procedure. The model of the beam is a Gaussian beam truncated by an aperture and weakly affected by comatic aberration. This model has been validated in previous contributions.[8]

Then, a two dimensional scan is made over the infrared antenna, that has been previously located at the position of the focal point of the lens. The scans analyzed in this contribution are consisted of

100 X 100 points taken every one micron. Some 2D scans are taken from the same device. After properly centered in the same position, a PCA analysis is made again. The method produces two different structures with different level of correlation. One of the structures is interpreted as the 2D scan. The other one corresponds with the noise introduced by the thermal instability of the infrared laser.[9,12] Applying the rectification process, this last structure is filtered from the original 2D scan map. After that, a single 2D scan is produced averaging the individual ones.

From this map and the beam shape model, it is possible to obtain the spatial response map through a deconvolution method. The iterative algorithm used to deconvol the signal is the so-called Lucy-Richardson algorithm. This algorithm takes a series of deconvolution steps in order to reproduce faithfully the original signal. The necessary number of steps can be evaluated through the use of the PCA: the noise in the signal is given by the rectification process. Then, the deconvolution method can be stopped when the accuracy in the reproduction of signal is equal or lower to the level of noise.
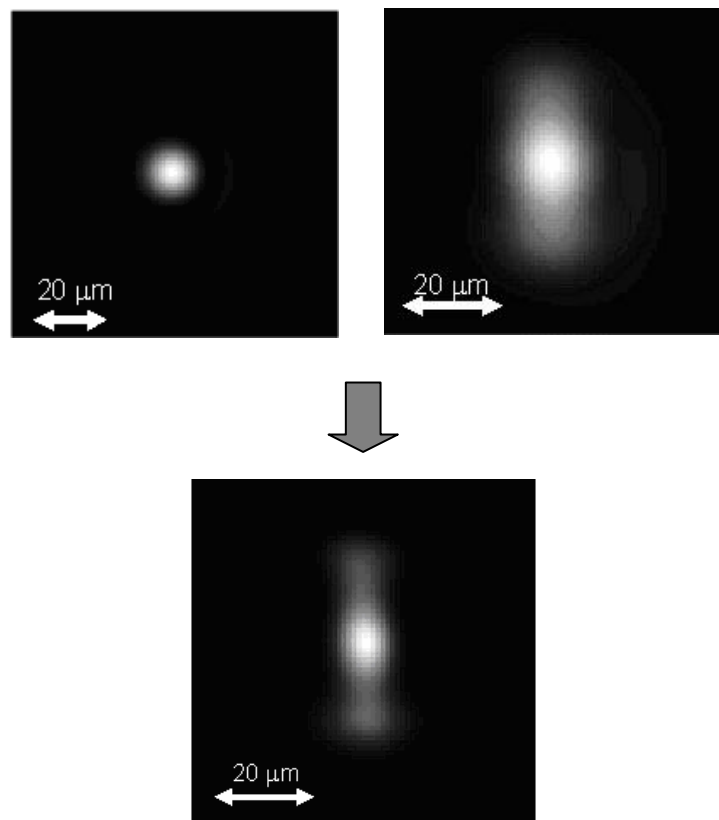

Figure 6: From the beam shape (Top left) and the 2D scan map (Top right) is it possible to obtain the spatial response map through a deconvolution process

3.4 Electrical efficiency

The maximum voltage given by the device was 6 mV (this figure is obtained from the lock-in amplifier and includes all the amplification electronics). This value is noted as V_0. Because the incoming power was mechanically modulated, the dissipated power is calculated as:

$$P_{dis} = \frac{1}{2} \frac{V_0^2}{R} \qquad (6)$$

Where R is the resistance of the device. The first step is the calculation of the optical power coupling N as: [13]

$$N = \frac{\left| \langle \phi | \psi \rangle \right|^2}{\langle \phi | \phi \rangle \langle \psi | \psi \rangle} \qquad (7)$$

Where ϕ, ψ are the detector spatial response and beam shape. The product $\langle \phi | \psi \rangle$ is defined as:

$$\langle \phi | \psi \rangle = \int_{-\infty}^{+\infty} \int_{-\infty}^{+\infty} \phi \psi^* \, dx dy \qquad (8)$$

According to this, the optical coupling N is around 0.8050. That is, only 20% of the incoming radiation is not optically coupled to the detector. If we not make the spatial integration in the numerator of equation (7) we can get a map of this optical coupling. This map is shown in figure 4.
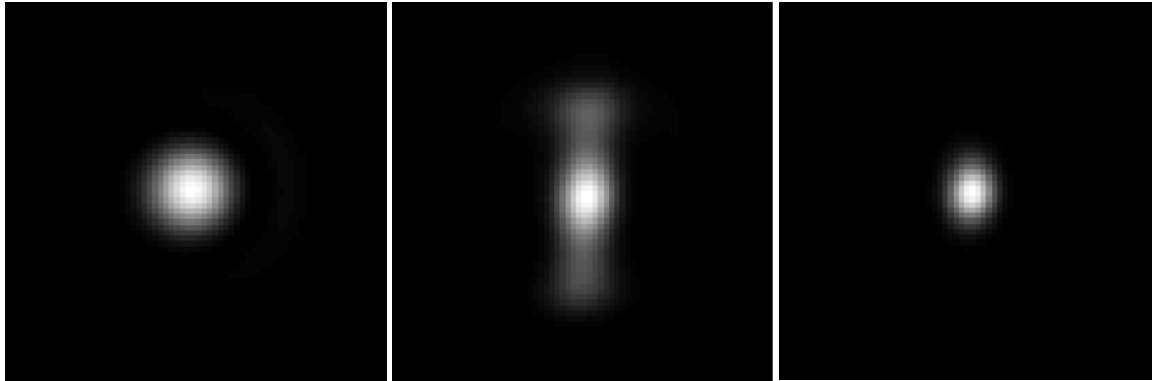

Figure 7: From left to right beamshape, detector spatial response and optical coupling.

From the previous NP_{dis} of the total energy is optically coupled to the detector. The electrical efficiency , η, is defined as:

$$\eta = \frac{P_{dis}}{NP} \tag{9}$$

This number represents the fraction of power optically coupled that it is finally dissipated in the resistance of the device and converted to an electrical signal. From the previous explanations this number is around $1.06 \cdot 10^{-5}$. There are some factors responsible for this number:

1. A high reflectivity of metals in infrared domain.
2. A low conductivity.
3. The transfer of dissipate heat produced in the antenna to the bolometer.

Additional studies are still pending about how to evaluate the weight of them into the electrical efficiency.

Measurements with another type of set up have been made. In this case the optical system used has a high F# in order to produce a large focalization region. This makes easy the alignment of the detector. Moreover, from the previous section, the electrical efficiency can depend on reflectivity and heat dissipation. These factors can depend on the beam used to take the measurements. In figure 8 is shown the beam shape in horizontal and vertical directions after using the analysis described in previous subsections. The beam size is very large, around 0.8 mm. The result for N is 0.33, much lower than in the F#1 configuration
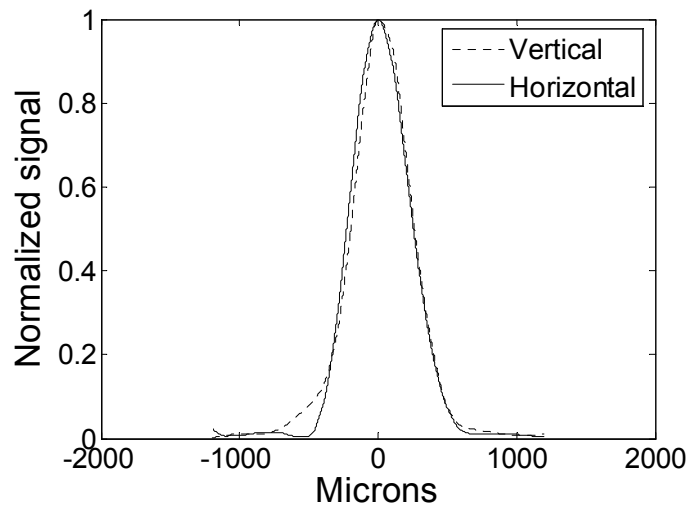

Figure 8: Beam profile in vertical and horizontal directions for the high F# configuration.

The dissipated power is calculated in the same way of section 2. The signal of detector has an averaged value of 1.276 mV. The resistance is assumed to be the same. Then, the electrical efficiency is $7.41 \cdot 10^{-7}$, less than in the previous case. This results reveals a non linear connection between optical coupling and electrical efficiency.

4. Conclusions.

A review of different aspects of infrared antennas metrology is presented. The measurements of these devices are mainly affected by noise coming from different sources: uncertainties in the power of the optical radiation, fluctuations of the signal in the infrared laser, electronic noise, small signal to noise ratio and so on. In this paper we have presented a general approach to this type of measurements taking into account the different sources of uncertainty. A Principal Component Analysis is extensively used in order to use the correlation in the signal to filter the noise while preserving important information. Measurements of the polarization response, the signal transfer response, and the spatial response and electric efficiency are presented with examples of different systems.

References

1. J. Alda, J. M. Rico-Garcia, J. M. López-Alonso, G. Boreman "Optical antenas for nano-photonic applications", Nanotechnology **16**, S230-S234 (2005).
2. F. J. González and G.D. Boreman, "Comparison of dipole, bowtie, spiral and log-periodic IR antennas," Infrared Phys. Technol., **46**, 418-428, (2005).
3. F. J. González, M. A. Gritz, C. Fumeaux, and G. D. Boreman, "Two dimensional array of antenna-coupled microbolometers," Int. J. Infrared Mil. Wav., **23**, 785-797, (2002).
4. F. J. González, B. Ilic, J. Alda, G. D. Boreman, "Antenna-coupled infrared detectors for imaging applications," IEEE J. Sel. Top. Quant. Electron., **11**, 117-120, (2005).
5. M. Y. Frankel, S. Gupta, J. A. Valdmanis and G. A. Mourou, "Terahertz, Attenuation and Dispersion Characteristics of Coplanar Transmission Lines", IEEE Trans MTT **39**, 910-916, (1991).
6. T. Mandviwala, B. Lail, G. Boreman "Infrared-frequency coplanar striplines: design, fabrication and measurements" Micro. Opt. Technol. Lett., **47**, 17-20 (2005).
7. I. Codreanu, F. J. González, G. D. Boreman, "Detection Mechanisms in microstrip antenna-coupled infrared detectors," Infrared Phys. Technol., **44**, 155-163, (2003).
8. J. Alda, C. Fumeaux, I. Codreanu, J. Schaefer, G. Boreman, "A deconvolution method for two-dimensional spatial-response mapping of lithographic infrared antennas," Appl. Opt., **38**, 3993-4000, (1999).
9. J. M. López-Alonso, B. Monacelli, J. Alda, and G. D. Boreman, "Infrared laser beam temporal fluctuations: characterization and filtering," Opt. Eng., **44**, 054203 (2005).
10. J. M. López-Alonso, J. Alda, E. Bernabeu "Principal component characterization of noise for infrared images" Appl. Opt., **41**, 320-331 (2002).
11. J. M. López-Alonso, J. Alda "Bad pixel identification by means of the principal component analysis" Opt. Eng. 41, 2152-2157 (2002).
12. J. M López-Alonso, B. Monacelli, J. Alda, G. Boreman, "Uncertainty Analysis in the measurement of the spatial responsivity of infrared antennas" Appl. Opt., **44**, 4557-4568 (2005).
13. J. Lesurf, Millimetre-Wave optics, devices and systems, Chapter 3, Adam Hilger ed. Bristol (1990).